Disruption of Lipid Uptake in Astroglia Exacerbates Diet-Induced Obesity

Yuanqing Gao,[1,2] Clarita Layritz,[1] Beata Legutko,[1] Thomas O. Eichmann,[3] Elise Laperrousaz,[4] Valentine S. Moullé,[4] Celine Cruciani-Guglielmacci,[4] Christophe Magnan,[4] Serge Luquet,[4] Stephen C. Woods,[5] Robert H. Eckel,[6] Chun-Xia Yi,[1,2] Cristina Garcia-Caceres,[1] and Matthias H. Tschöp[1]

Diabetes 2017;66:2555–2563 | https://doi.org/10.2337/db16-1278

Neuronal circuits in the brain help to control feeding behavior and systemic metabolism in response to afferent nutrient and hormonal signals. Although astrocytes have historically been assumed to have little relevance for such neuroendocrine control, we investigated whether lipid uptake via lipoprotein lipase (LPL) in astrocytes is required to centrally regulate energy homeostasis. Ex vivo studies with hypothalamus-derived astrocytes showed that LPL expression is upregulated by oleic acid, whereas it is decreased in response to palmitic acid or triglycerides. Likewise, astrocytic LPL deletion reduced the accumulation of lipid droplets in those glial cells. Consecutive in vivo studies showed that postnatal ablation of LPL in glial fibrillary acidic protein–expressing astrocytes induced exaggerated body weight gain and glucose intolerance in mice exposed to a high-fat diet. Intriguingly, astrocytic LPL deficiency also triggered increased ceramide content in the hypothalamus, which may contribute to hypothalamic insulin resistance. We conclude that hypothalamic LPL functions in astrocytes to ensure appropriately balanced nutrient sensing, ceramide distribution, body weight regulation, and glucose metabolism.

Metabolic homeostasis is regulated by a complex central nervous system (CNS) network that senses and integrates nutrient and hormonal signals from the periphery to regulate feeding behavior, energy expenditure, and glucose homeostasis. Considerable evidence indicates that lipid sensing by the brain is a normal component of such regulation (1–6). The mechanism underlying the role of lipid sensing by the brain in metabolism has recently attracted considerable interest in the metabolic field.

Glial cells constitute around 50% of the total cells in the whole brain (7), but these have historically received less attention in metabolic research. Astrocytes are the most abundant and diverse glial cells; they are the primary cell population in the brain that synthesizes and metabolizes lipids (8,9), positioning them as major players in the regulation of lipid sensing and metabolism in the CNS. Consistent with this, fatty acid oxidation in the brain occurs primarily in astrocytes, although at a very low rate compared with glycolysis (8,10). In addition, chronic consumption of a high-fat diet (HFD) results in both hyperlipidemia and hypothalamic astrogliosis (11). Until now, however, the functional significance of astrocyte lipid metabolism in CNS metabolic regulation has been unknown.

Lipoprotein lipase (LPL), the key enzyme required to hydrolyze triglycerides (TGs), has been implicated in CNS metabolic regulation (12). LPL is the "gatekeeper" for lipids in peripheral tissues, modulating the distribution of fatty acids derived from TG-rich lipoproteins (13). Importantly, LPL is regulated by nutrients and hormones in a tissue-specific manner (14). LPL expression and enzyme activity have been detected in both neurons and glial cells in the

[1]Helmholtz Diabetes Center (HDC) and German Center for Diabetes Research (DZD), Helmholtz Zentrum München and Division of Metabolic Diseases, Department of Medicine, Technische Universität München, Munich, Germany
[2]Department of Endocrinology and Metabolism, Academic Medical Center, University of Amsterdam, Amsterdam, the Netherlands
[3]Institute of Molecular Biosciences, University of Graz, Graz, Austria
[4]Unité de Biologie Fonctionnelle et Adaptative, Sorbonne Paris Cité, CNRS UMR 8251, University of Paris Diderot, Paris, France
[5]Department of Psychiatry and Behavioral Neuroscience, University of Cincinnati, Cincinnati, OH
[6]Division of Endocrinology, Metabolism, & Diabetes, University of Colorado at Denver, Denver, CO

Corresponding author: Matthias H. Tschöp, tschoep@helmholtz-muenchen.de.

Received 20 October 2016 and accepted 4 July 2017.

This article contains Supplementary Data online at http://diabetes.diabetesjournals.org/lookup/suppl/doi:10.2337/db16-1278/-/DC1.

brain (12,15–17). However, the functional significance of LPL in astrocytes is unknown.

In this study, we investigated the function of LPL in astrocytes in lipid metabolism in the brain and potential contributions of astrocytic LPL to diet-induced obesity. We found that LPL is responsible for controlling cellular lipid storage in astrocytes. In a loss-of-function study, mice lacking LPL uniquely in astrocytes had glucose intolerance and accelerated body weight gain when maintained on an HFD. We also found increased ceramide content in the hypothalamus of astrocytic LPL–deficient mice, accompanied by increased microglial reactivity and endoplasmic reticulum (ER) stress. Collectively, our data imply that LPL in astrocytes mediates lipid partitioning in the brain and is required for the CNS to appropriately sense nutrients and regulate energy homeostasis.

RESEARCH METHODS AND DESIGN

Animals

All studies were approved by and performed according to the guidelines of the Institutional Animal Care and Use Committees of the University of Cincinnati and the Helmholtz Center Munich, Bavaria, Germany. All mice were housed in groups under a 12-h light/12-h dark cycle at 23°C, with free access to food and water. Mice were fed either a standard chow diet or an HFD (D12331; Research Diets).

Astrocyte-specific postnatal LPL-knockout mice (GFAP-LPL$^{-/-}$) were generated by crossing LPL$^{lox/lox}$ mice (18) with hGFAP-CreER^{T2}, transgenic mice harboring the tamoxifen-inducible Cre recombinase driven by a human glial fibrillary acidic protein (hGFAP) promoter (19). At the age of 6 weeks, 100 μg tamoxifen was given by i.p. injection daily for five consecutive days. LPL loxP-homozygous and Cre-positive mice were used to generate knockout mice (GFAP-LPL$^{-/-}$). Their littermates, which were LPL loxP homozygous but Cre-negative, served as wild-type controls (GFAP-LPL$^{+/+}$).

For the flow cytometry study and the in situ hybridization study, GFAP-LPL$^{+/+}$ and GFAP-LPL$^{-/-}$ mice were crossed with hGFAP-EGFP reporter mice (20) in order to label the Cre-targeted cells with an EGFP tag. To evaluate the efficiency of the postnatal deletion in different brain regions, GFAP-LPL$^{+/+}$ mice were crossed with Rosa26 ACTB-tdTomato reporter mice and received the same tamoxifen injections as the experimental group. To evaluate the presence of ceramide in microglia, we used microglia–green fluorescent protein (GFP) reporter mice (Jax mice 005582).

Hypothalamic Primary Culture

For astrocytes, hypothalami were isolated from 2-day-old C57BL6J mice and triturated in minimum essential medium containing 1% penicillin-streptomycin, 10% FCS, and 5.5 mmol/L glucose. The cell pellet was centrifuged, resuspended, and seeded in a 175-cm^3 cell culture flask. After 8–9 days, the mixed glial culture reached 90% confluence. Then the flasks were placed in a shaking incubator (240 rpm at 37°C) overnight to remove microglia. The cells were then seeded for the experiments.

For neurons, the hypothalami were isolated from 14-day-old embryos. After tripsinization, single cells were plated on 12-well plates and cultured in neurobasal medium supplemented with B-27 and GlutaMAX I. After 7 days in the culture, the presence of glia cells was efficiently reduced by adding the mitotic inhibitor Ara C (cytosine-1-β-D-arabinofuranoside), and hypothalamic neurons started to develop synaptic processes. Cells were then harvested and stored at −80°C until RNA extraction.

Adenovirus Cre-Mediated Deletion of LPL in Hypothalamic Astrocyte Cultures

To induce the ex vivo ablation of LPL, primary hypothalamic astrocytes were obtained from LPL$^{lox/lox}$ mice and were seeded in six-well cell culture plates, as described above. Once they reached 90% confluence, astrocytes were transfected with adeno-Cre and adeno-control viruses (Vector Biolabs) plus 1% adenoBOOST (ATCGbio Life Technology) for 4 h to generate astrocyte cultures with LPL (Astro-LPL$^{+/+}$) or without LPL (Astro-LPL$^{-/-}$).

Seahorse Analysis

Astrocytes were seeded in an XF24 plate (Seahorse Bioscience) with 80,000 cells/well. After 24 h of adeno-Cre or adeno-control virus transfection, cells were washed with PBS and incubated with XF assay medium containing 5.5 mmol/L glucose in a 37°C air incubator for 1 h. The XF24 plate was then transferred to a temperature-controlled (37°C) extracellular flux analyzer (Seahorse Bioscience) and subjected to an equilibration period. To analyze extracellular acidification rates derived from glycolysis, the measurement periods were ended by adding 2-deoxy-glucose (100 mmol/L). 2-Deoxy-glucose-sensitive proton production rate estimates the ATP production from glycolysis at a 1:1 ratio (1 pmole/min proton = 1 pmole/min ATP). To normalize respirometry readings to the number of cells per well, cells were stained with crystal violet after the flux experiment. L-Lactate from the astrocyte culture medium was assayed with an EnzyChrom L-Lactate Assay Kit (BioAssay Systems).

Lipase Activity Assay

Cells were collected in 20 mmol/L Tris and 150 mmol/L NaCl with 15 μg/mL heparin. After sonication, cell lysates were kept at 37°C for 45 min, followed by 10,000*g* centrifugation at 4°C for 10 min. Lipase activity was determined by a fluorometric LPL activity assay kit (STA-610-CB; Cell Biolabs Inc.). Protein level was determined by a Pierce BCA Protein Assay kit (Thermo Fisher). Lipase activity was normalized to protein content.

Real-time PCR

To analyze gene expression, hypothalamic tissue was harvested and total RNA was isolated using an RNeasy Lipid Tissue Kit (Qiagen). After reverse transcription by a QuantiTect Reverse Transcription Kit (Qiagen), gene expression was analyzed by real-time PCR with TaqMan probes (Applied Biosystems) and SYBR primers. Hypoxanthine phosphoribosyltransferase 1 (*Hprt*) was used as a

housekeeping gene. Information about the sequences can be found in Supplementary Table 1.

PCR

For PCR to detect the LPL δ band after Cre-loxP recombination, the following primer sequence was set: forward, 5′-CGCCCTGGAACATCACTAAT-3′; reverse, 5′-CTTCTCAATTGT GGGCAGGT-3′. The primers would develop a band of ~2,000 bp on the wild-type DNA sequence and an LPL δ band of 409 bp after floxed sequences cut by Cre.

Flow Cytometry

The isolation protocol has been described in detail before (21). Briefly, the forebrain was dissected and dissociated using enzymatic and mechanical approaches. Single cells were separated by a sucrose gradient. Cells were sorted using a flow cytometry cell sorter (FACS Aria l; BD Biosciences) with FACS Diva software, based on GFP signals. Purified GFAP-expressing astrocytes from GFAP-LPL$^{+/+}$ and GFAP-LPL$^{-/-}$ mice were used to validate the LPL knockdown using real-time PCR, as described above.

Glucose Tolerance Test

An intraperitoneal glucose tolerance test was performed by injecting glucose (2 g/kg, 25% w/v *d*-glucose; Sigma) in 0.9% w/v NaCl after a 5-h fast. Tail blood glucose levels (milligrams per deciliter) were measured with a TheraSense Freestyle glucometer (Abbott Diabetes Care) before (0 min) and 15, 30, 60, and 120 min after injection.

Feeding Experiments and Metabolic Phenotyping

Body weight was measured weekly throughout the study. Food intake was measured on a daily basis for 2 weeks at the end of the study. Animals were double-housed, and daily food intake of mice in each cage was measured and averaged to a per-mouse per-day equivalent. Energy expenditure and physical activity were measured using a customized indirect calorimetric system (TSE Systems). Mice were adapted to the system for 24 h before data were collected over the following 4 days.

Immunohistochemistry and Image Analysis

Immunohistochemistry was carried out as described before (22). Briefly, mice were perfused and fixed with 4% paraformaldehyde in 0.1 mol/L PBS (pH 7.4) at 4°C. After being equilibrated for 48 h with 30% sucrose in Tris-buffered saline, coronal sections (30 μm) were cut on a cryostat. Sections were washed and incubated overnight with primary antibodies at 4°C: rabbit anti-GFAP (Dako; Agilent), rabbit anti-iba1 (ionized calcium-binding adapter molecule 1; Synaptic Systems), mouse anticeramide (Enzo Life Sciences), rabbit anti-NeuN (Cell Signaling Technology). On the second day, sections were rinsed and incubated with biotinylated secondary antibodies and an avidin-biotin complex (Vector Laboratories). The reaction product was visualized by incubation in 1% diaminobenzidine with 0.01% hydrogen peroxide. For immunofluorescence, sections were incubated with corresponding ALEXA fluorescent secondary antibodies (Jackson ImmunoResearch Labs).

Immunoreactivity was analyzed with ImageJ software. An appropriate color threshold for 3,3′-diaminobenzidine staining was set up manually for the first picture and applied to all subsequent pictures. The brain area covered by the 3,3′-diaminobenzidine staining signals (iba1, GFAP, and agouti-related peptide [AGRP]) above the color threshold of each individual brain section in the fixed hypothalamic region was used to quantify immunoreactivity. Two brain sections (at a similar anatomical level) from each individual animal were used to calculate the immunoreactivity average of each animal.

In Situ Hybridization

For in situ hybridization, 30-μm thick coronal brain sections were treated with 2 μg/mL proteinase K at 37°C for 30 min, 0.2% glycine buffer for 30 s, and 0.1% Triton X-100 for 10 min. Brain sections were hybridized in hybridization buffer (Sigma-Aldrich) containing 200 nmol/L locked nucleic acid–modified cDNA probes labeled with digoxigenin (5′-TGGAACTACTTCTCTAACATAT-3′) (Exiqon) at 52°C overnight. After stringent washing in sodium chloride–sodium citrate buffer at 52°C and a final wash in 0.1 M PBS, the sections were coincubated with goat anti-digoxigenin antibody (Abcam) and chicken anti-GFP (Acris) at 4°C overnight. Sections were incubated with biotinylated antichicken secondary antibody for 1 h and then incubated with streptavidin conjugated with DyLight 488 (for GFP) and rabbit antichicken antibody conjugated by DyLight 647 (for digoxigenin) (all from Jackson ImmunoResearch Labs). After a thorough rinse, the sections were mounted with mounting medium and visualized by confocal microscopy (Zeiss-LSM710).

Untargeted Lipidomic Analysis of Ceramide Species

Total lipids of weighed hypothalamus preparations were extracted twice according to the process described by Folch et al. (23), using chloroform/methanol/water (2:1:0.6, v/v/v) containing 500 pmol butylated hydroxytoluene, 1% acetic acid, and 4 nmol C17-ceramide as the internal standard (Avanti Polar Lipids) per sample. Combined organic phases of the double extraction were dried under a stream of nitrogen and dissolved in 200 μL chloroform/methanol/2-propanol (2:1:12, v/v/v) for ultraperformance liquid chromatography quadrupole time of flight analysis (UPLC-qTOF). Chromatographic separation was performed using an AQUITY UPLC System (Waters), equipped with an HSS T3 column (2.1 × 100 mm, 1.8 μm; Waters), as previously described (24). A SYNAPT G1 HDMS qTOF mass spectrometer (Waters) equipped with an electrospray ionization source was used for detection. Data were acquired using MassLynx 4.1 software (Waters). Ceramides were analyzed with Lipid Data Analyzer 1.6.2 software. Extraction efficacy and lipid recovery were normalized using internal standards.

Statistical Analysis

All statistical analyses were performed using GraphPad Prism software. Two groups were compared using a two-tailed, unpaired Student *t* test. Two-way ANOVA was performed to detect significant interactions between genotype

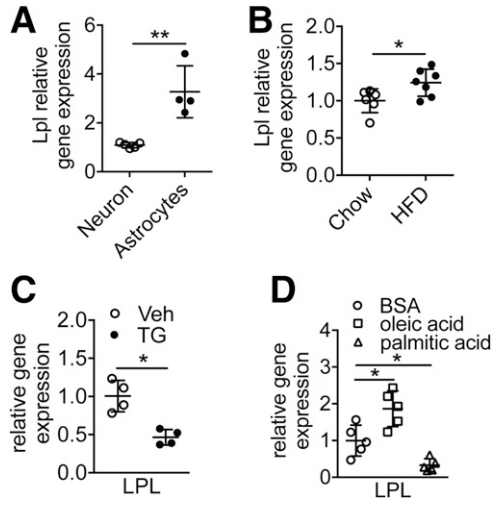

Figure 1—Astrocytic LPL is regulated by nutrients in the hypothalamus. LPL expression in primary isolated hypothalamic neurons and astrocytes (white circles, neurons; black circles, astrocytes) (*A*) and the hypothalami of mice fed an HFD for 8 months (white circles, chow; black circles, HFD) (*B*). In primary astrocytes, LPL expression levels were modulated by a 0.02% TG emulsion (black circles, TG) (*C*) and 50 μmol/L oleic acid (squares), palmitic acid (triangles), or BSA (vehicle, white circles) (*D*). **P* < 0.05, ***P* < 0.01 (*n* = 4–7 mice/group).

and diet, and multiple comparisons were analyzed after Bonferroni post hoc tests. *P* values <0.05 were considered significant. All results are presented as means ± SDs when *n* <10 and as means ± SEMs when *n* >10.

RESULTS

Astrocytic LPL Is Regulated by Nutrients in the Hypothalamus

LPL activity has been detected in the hypothalamus, and changes occur in response to a prolonged fast (25). We first confirmed the presence of LPL in the hypothalamus, particularly in primary astrocytes, and its modulation in response to different nutrient stimuli. Consistent with previous reports, LPL was expressed by both neurons and glial cells (12,26). We compared the relative abundance of LPL in primary isolated hypothalamic neurons and astrocytes and found higher levels of LPL-enriched mRNA in astrocytes than in neurons (Fig. 1*A*). Next we evaluated the impact of exposure to lipid on LPL expression in vivo and in vitro. An increase in LPL mRNA levels was observed in the hypothalami of mice fed an HFD for 8 months (Fig. 1*B*). When hypothalamus-derived astrocytes were exposed to TGs and palmitic acid, LPL expression was reduced, whereas the opposite effect was seen with oleic acid (Fig. 1*C* and *D*). These data suggest that astrocytic LPL is regulated by nutrients and responds differentially to saturated and nonsaturated fatty acids.

Loss of LPL Reduces Cellular Lipid Content and Increases Glycolytic Capacity in a Hypothalamic Astrocyte Culture

To analyze whether LPL in astrocytes regulates cellular lipid accumulation and glucose metabolism, we isolated

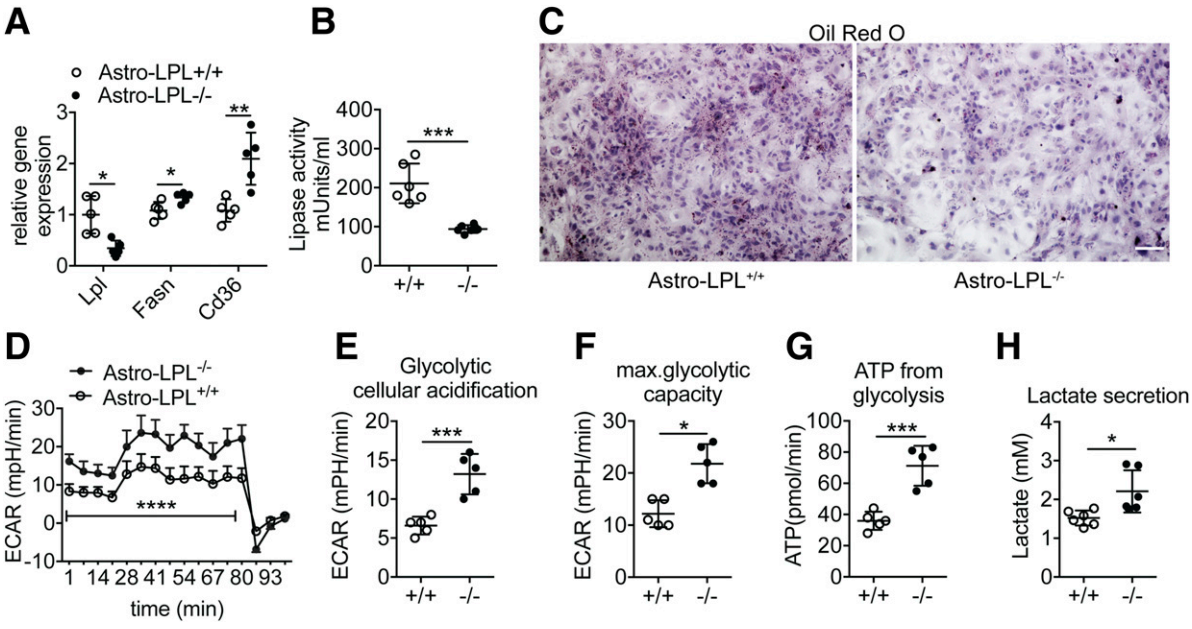

Figure 2—The loss of LPL reduces cellular lipid content and increases glycolytic capacity in hypothalamic astrocyte cultures. Astrocytes were isolated from hypothalami of LPL-flox mice and transfected with an adeno-GFP or adeno-Cre virus to obtain astrocytes with LPL (Astro-LPL$^{+/+}$) or without LPL (Astro-LPL$^{-/-}$). The loss of LPL in astrocyte cultures induced changes in the expression of LPL, fatty acid synthase (Fasn), and cluster of differentiation 36 (Cd36) (*A*); lipase activity (*B*); and lipid content in astrocytes stained with Oil Red O (*C*). Scale bar = 50 μm. Seahorse analysis demonstrated that Astro-LPL$^{-/-}$ cells had enhanced glycolysis (*D* and *E*), increased mitochondrial glycolytic capacity (*F*), and increased ATP production from glycolysis (*G*). Lactate secretion was also higher in Astro-LPL$^{-/-}$ cells than in Astro-LPL$^{+/+}$ cells (*H*). White circles, Astro-LPL$^{+/+}$; black circles, Astro-LPL$^{-/-}$. **P* < 0.05; ***P* < 0.01; ****P* < 0.001; *****P* < 0.0001 (*n* = 5–6 mice/group). ECAR, extracellular acidification rate; max., maximum.

hypothalamic astrocytes from LPL$^{lox/lox}$ mice and performed virus-mediated excision of LPL by in vitro transfection with Cre-expressing adenoviruses (AAV-Cre) in order to finally obtain Astro-LPL$^{+/+}$ and Astro-LPL$^{-/-}$ cells. Reduced LPL expression (Fig. 2*A*) and lipase activity (Fig. 2*B*) were confirmed by quantitative PCR and a lipase activity assay, respectively, after virus transfection. Loss of LPL activity leads to a decrease of lipid droplet content in astrocytes, as assessed by Oil Red O staining (Fig. 2*C*). Lipogenesis-related genes, including cluster of differentiation 36 and fatty acid synthase, were upregulated in LPL-deficient astrocytes (Fig. 2*A*), indicating a compensatory response to the lipid-derived situation. We next determined whether LPL regulates glycolysis in astrocytes (Fig. 2*D*). Indeed, Astro-LPL$^{-/-}$ cells had increased cellular acidification and maximal glycolytic capacity (Fig. 2*E* and *F*). More ATPs were produced from enhanced glycolysis in these cells than in Astro-LPL$^{+/+}$ cells (Fig. 2*G*). Accordingly, lactate secretion was increased in the medium from Astro-LPL$^{-/-}$ cells (Fig. 2*H*), consistent with the increased glycolysis. These data indicate that LPL participates in regulating lipid content and energy metabolism in astrocytes. Specifically, we found that the lack of LPL reduces astrocytic lipid storage and enhances astrocytic glycolysis.

Validation of Postnatal Ablation of LPL in GFAP-Expressing Cells in the Brain

To evaluate the impact of the loss of LPL in astrocytes in vivo, we generated postnatal astrocyte–specific LPL-knockout mice using the Cre/lox system. We first validated the deletion of LPL in astrocytes after peripheral tamoxifen injection at 6 weeks of age, using multiple approaches. We confirmed the Cre-driven deletion of LPL in hGFAP-positive cells by in situ hybridization (Fig. 3*A*). Primers were designed based on genetic construction of LPL-floxed sequences to detect a specific band after Cre-induced recombination (Fig. 3*B*). Purified GFAP-expressing astrocytes were sorted from the brains of GFAP-LPL$^{+/+}$ mice (LPL$^{lox/lox}$ mice injected with tamoxifen) or GFAP-LPL$^{-/-}$ mice (hGFAP-CreER^{T2}-LPL$^{lox/lox}$ mice injected with tamoxifen), which were crossed with hGFAP-EGFP reporter mice. Quantitative PCR of sorted GFP-expressing brain cells confirmed the knockdown of LPL (Fig. 3*C*). Using Rosa26 ACTB-tdTomato reporter mice, which were crossed with GFAP-LPL$^{-/-}$ mice, we confirmed that Cre-mediated postnatal ablation occurred in the brain after tamoxifen injection (Supplementary Fig. 1*A*). The majority of the Cre-recombined GFAP-expressing astrocytes were located in the hypothalamus (46.3% ± 2.1%) in comparison with other brain regions such as the thalamus, hippocampus, and cortex (Fig. 3*D*). Even though peripheral tissues also express GFAP, including stellate cells in the liver and pancreas (27,28), no alterations in LPL expression were found in the livers of GFAP-LPL$^{+/+}$ and GFAP-LPL$^{-/-}$ mice (Fig. 3*E*). Glucose-induced insulin secretion in isolated islets was also not affected between groups (Fig. 3*F*). These findings confirm that the loss of LPL occurs specifically in GFAP-expressing cells in the brain.

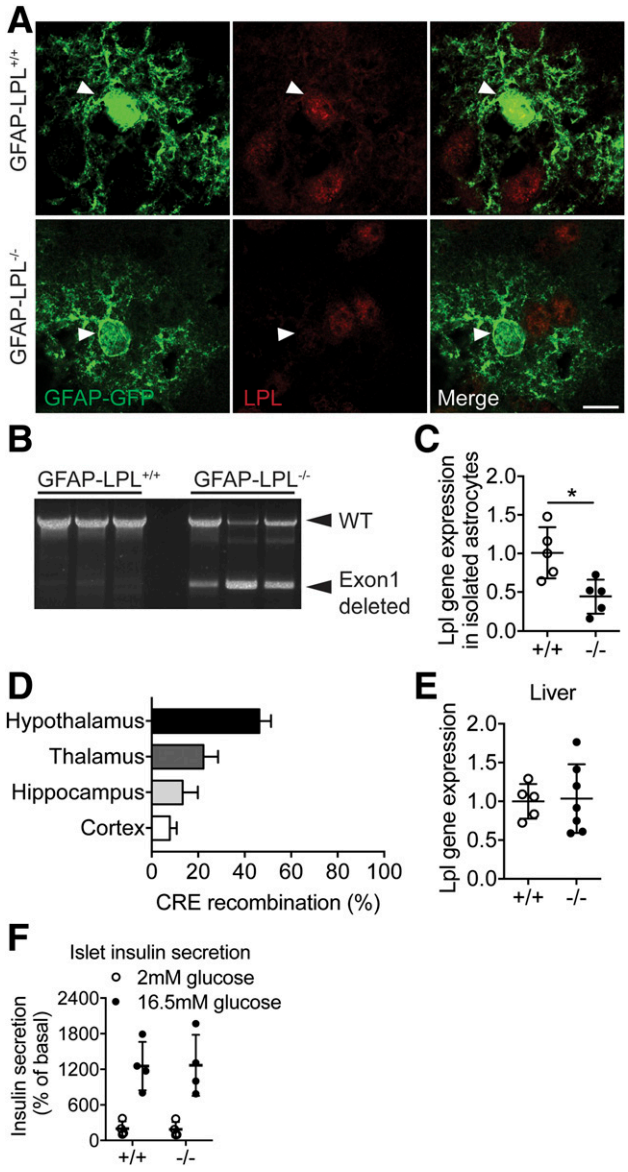

Figure 3—Validation of postnatal ablation of LPL in GFAP-expressing cells in mouse brains. Astrocyte-specific LPL postnatal knockout mice were achieved by crossing GFAP-CreER$^{T2+/-}$ mice with LPL flox$^{+/+}$ mice. After tamoxifen injection at 6 weeks of age, LPL deletion was confirmed by in situ hybridization (arrowheads, targeted astrocyte) (scale bar = 10 μm) (*A*), PCR using DNA sequences after Cre-mediated deletion of exon 1 in the LPL gene (*B*), and quantitative PCR from purified GFAP-positive astrocytes isolated by flow cytometry from GFAP-LPL$^{+/+}$ (white circles) and GFAP-LPL$^{-/-}$ (black circles) mice (*C*). The efficiency of Cre-mediated recombination was evaluated by crossing GFAP- LPL$^{+/+}$ mice with Rosa26 ACTB-tdTomato reporter mice and measuring the ratio between Cre-recombined astrocytes in different brain regions and the total Cre-recombined cells detected in slides of brain sections (*D*). No differences in LPL expression were found in the liver between GFAP-LPL$^{+/+}$ (white circles) and GFAP-LPL$^{-/-}$ (black circles) mice (*E*) or in ex vivo insulin secretion from isolated islets in response to glucose (white circles, 2 mmol/L glucose; black circles, 16.5 mmol/L glucose) (*F*). *$P < 0.05$, vs, Astro-LPL$^{+/+}$ (n = 4–5 mice/group).

Loss of LPL in Astrocytes Causes Ceramide Accumulation, Microglial Activation, and Increased AGRP in the Hypothalamus but Not in Other Brain Areas

It was previously reported that ceramide synthesis in the brain is associated with LPL activity (29). Ceramide is an important multifunctional intracellular signaling molecule. In the periphery, ceramide accumulation causes lipid toxicity and insulin resistance (30,31). In the mouse brain, after knocking out LPL from GFAP-positive astrocytes, total ceramide content was increased in the hypothalamus (Fig. 4*A*). Ceramide species with different acyl chains were also analyzed (Fig. 4*B*). Mice lacking astrocytic LPL had increased C18:0, C18:1, and C22:0 levels in the hypothalamus. Through ceramide staining, we also found that ceramide immunoreactivity–positive cells, which are mainly neurons (Supplementary Fig. 2), were markedly increased in the hypothalamus in GFAP-LPL$^{-/-}$ mice (Supplementary Fig. 1*B* and *C*), consistent with lipidomics results.

In accordance with several studies that reported that ceramide accumulation in the hypothalamus causes ER stress and interrupts energy balance (32), we observed that a loss of LPL in astrocytes increased the expression of several markers of ER stress in the hypothalamus. Specifically, we found that chaperone glucose-regulated protein 78 kDa and total and sliced X-box binding protein 1 were each increased in the hypothalamus of GFAP-LPL$^{-/-}$ mice (Fig. 4*C*), whereas these were unchanged in the hippocampi or cortexes of those mice (Supplementary Fig. 1*F* and *G*).

We also analyzed the effect of the loss of LPL in astrocytes using immunohistochemistry. GFAP immunoreactivity did not differ between GFAP-LPL$^{+/+}$ and GFAP-LPL$^{-/-}$ mice (Fig. 4*D* and *E*). However, the major immune-responsive cells—microglia—had increased reactivity in the medial

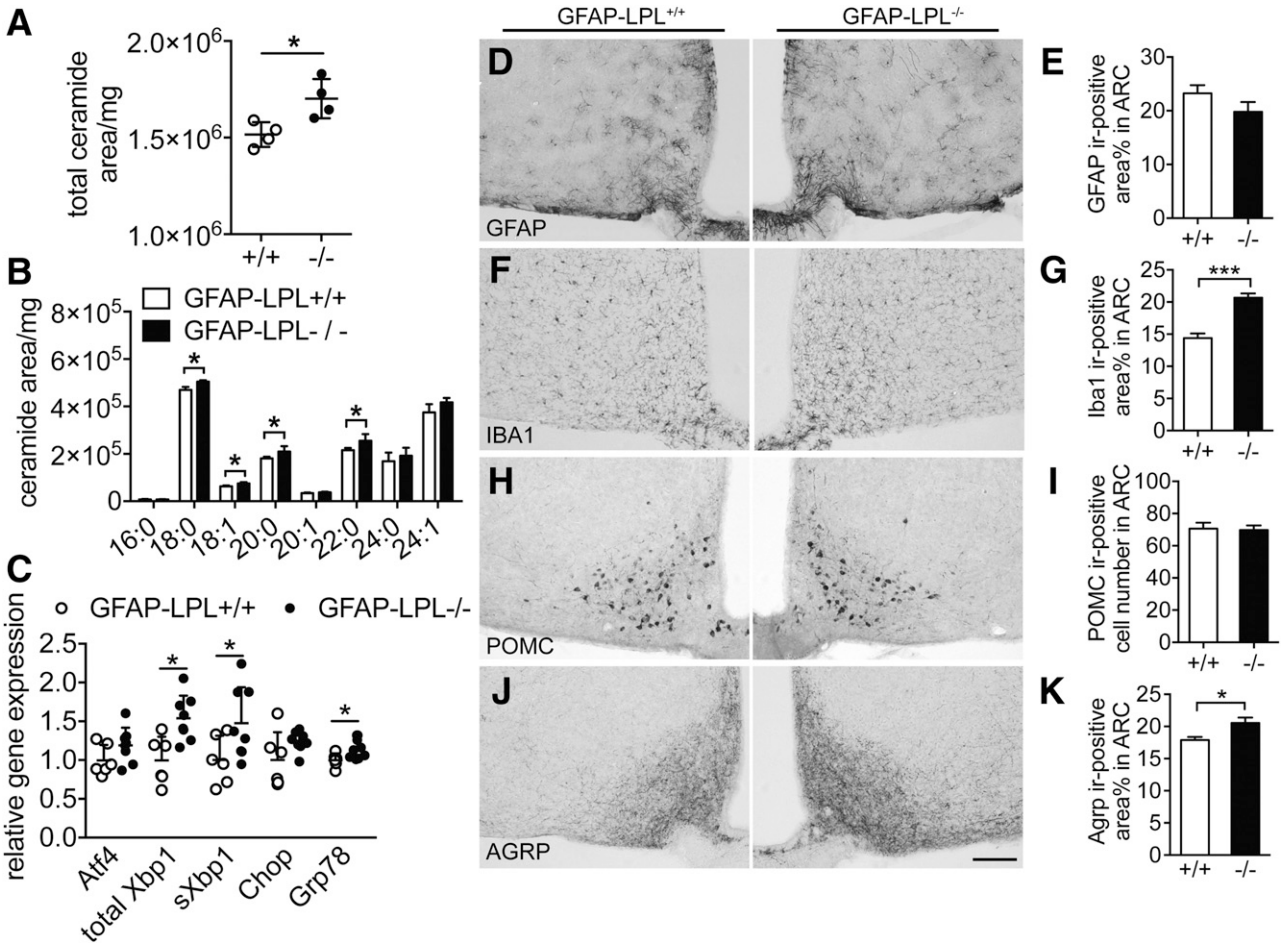

Figure 4—The loss of LPL in astrocytes causes ceramide accumulation, ER stress, and increased immunoreactivity of Iba1 and AGRP in the hypothalamus. Total ceramide content (*A*) and acyl-chain ceramide species (*B*) in the hypothalami of GFAP-LPL$^{+/+}$ and GFAP-LPL$^{-/-}$ mice were determined by lipidomics (n = 4 mice/group). *C*: The expression of markers of ER stress was examined in the hypothalami of GFAP-LPL$^{+/+}$ and GFAP-LPL$^{-/-}$ mice (n = 6–8 mice/group). No differences were found in the reactivity of GFAP in the hypothalamus (*D* and *E*), whereas microglial (Iba1-positive cells) reactivity was increased in GFAP-LPL$^{-/-}$ mice (*F* and *G*) (n = 6–12 mice). POMC cell numbers did not change (*H* and *I*), whereas AGRP immunoreactivity was increased in the hypothalamus of GFAP-LPL$^{-/-}$ mice (*J* and *K*) (n = 6–12 mice). Scale bar = 100 μm. White circles, GFAP-LPL$^{+/+}$ mice; black circles, GFAP-LPL$^{-/-}$ mice. *P < 0.05; ***P < 0.001. ARC, arcuate nucleus; Atf4, activating transcription factor 4; Chop, C/EBP-homologous protein; Grp78, glucose-regulated protein 78 kDa; ir, immunoreactivity; Xbp1, X-box binding protein 1.

basal hypothalamus (Fig. 4*F* and *G*), but not in other brain regions (Supplementary Fig. 1*D* and *E*), of GFAP-LPL$^{-/-}$ mice, suggesting that microglia respond to ceramide-induced lipid toxicity and that this may contribute to hypothalamic insulin resistance and metabolic disorders. Such glial and ceramide alterations in the hypothalamus were associated with changes in specific neuronal populations involved in the regulation of energy balance: AGRP neurons and proopiomelanocortin (POMC) neurons. Although POMC cell number did not change (Fig. 4*H* and *I*), AGRP immunoreactivity was significantly elevated in the GFAP-LPL$^{-/-}$ mice (Fig. 4*J* and *K*).

Collectively, these data suggest that in the current model, a lack of LPL in astrocytes causes ceramide to accumulate in the hypothalamus and is associated with microglial activation, ER stress, and increased AGRP.

Mice Lacking LPL in Astrocytes Have Exaggerated Body Weight Gain and Glucose Intolerance When Maintained on an HFD

To assess whether the loss of LPL in astrocytes affects whole-body energy metabolism, mice were maintained on chow or an HFD for 10 weeks beginning at 10 weeks of age. Only modest metabolic phenotypes were initially observed when the animals were fed the chow diet (Supplementary Fig. 3). Briefly, GFAP-LPL$^{-/-}$ mice exhibited a glucose intolerance phenotype and reduced activation of AKT (phospho-AKT; phosphorylation in Ser 473 of protein kinase B) in the hypothalamus 10 min after peripheral insulin stimulation. Although the mice had a slightly higher food intake at 24 weeks of age than did GFAP-LPL$^{+/+}$ mice, no changes were detected in body weight or fat mass.

When fed an HFD, GFAP-LPL$^{-/-}$ mice had accelerated body weight gain (Fig. 5*A*) relative to that of controls; this was mainly as a result of increased fat mass (Fig. 5*B* and *C*). Calorimetric measurements after 10 weeks on the HFD revealed that GFAP-LPL$^{-/-}$ mice had increased food intake (Fig. 5*D*) and less locomotor activity (Fig. 5*F*), and these likely contributed to the higher body weight gain. Higher energy expenditure (Fig. 5*E*) might be a consequence of the higher body weights of GFAP-LPL$^{-/-}$ mice. Plasma leptin level was elevated in GFAP-LPL$^{-/-}$ mice (Fig. 5*G*), which was consistent with the increased fat mass. Plasma insulin level did not change (Fig. 5*H*). GFAP-LPL$^{-/-}$ mice had enhanced glucose intolerance (Fig. 5*I* and *J*). Because GFAP-LPL$^{-/-}$ mice consuming the chow diet already exhibited glucose intolerance without changes in body weight or fat mass, we determined that the genotype is a determinant of the glucose intolerance phenotype. In GFAP-LPL$^{-/-}$ mice maintained on the HFD, the increased adiposity exaggerates glucose intolerance. Thus, the loss of LPL in astrocytes induces glucose intolerance and exaggerated body weight when consuming an HFD, implying that LPL-related lipid metabolism in astrocytes has an important role in regulating metabolic homeostasis.

DISCUSSION

In the experiments described here, we investigated the function of LPL in astrocytes and its role in systemic

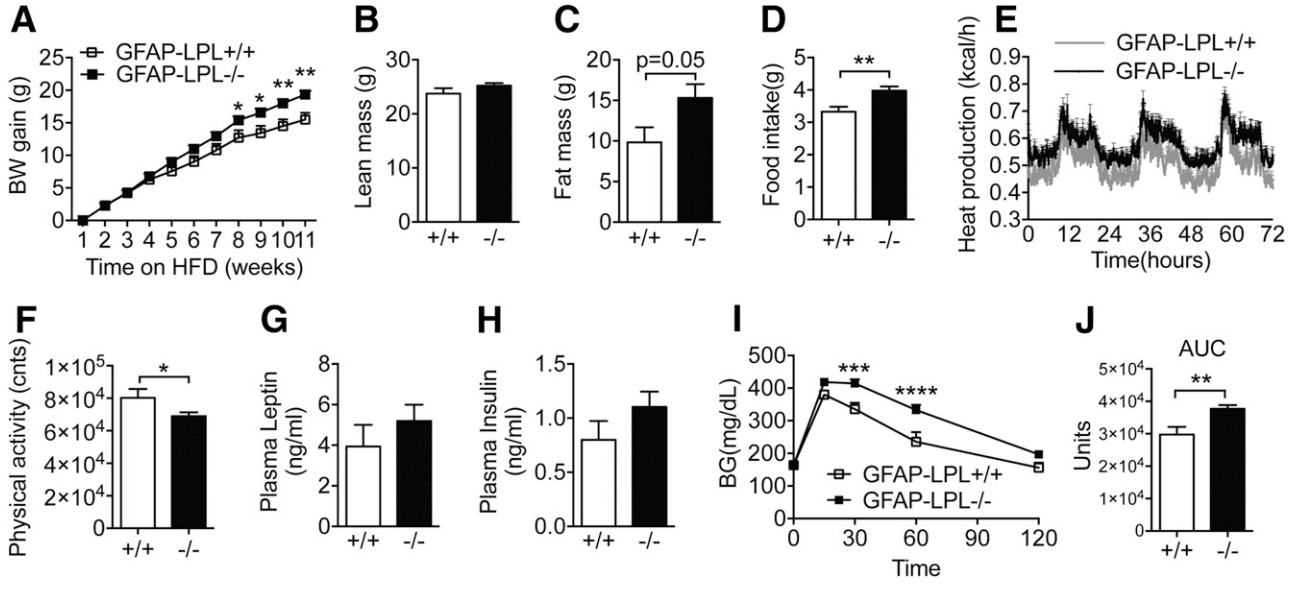

Figure 5—Mice lacking LPL in astrocytes have exaggerated body weight gain and glucose intolerance when maintained on an HFD. GFAP-LPL$^{-/-}$ mice fed an HFD had increased body weight (BW) gain (*A*), unchanged lean mass (*B*), increased fat mass (*C*), and increased daily food intake (*D*) compared with their GFAP-LPL$^{+/+}$ littermates. Calorimetric analysis demonstrated that GFAP-LPL$^{-/-}$ mice had higher energy expenditure (*E*) and less physical activity (*F*). Plasma leptin levels increased in GFAP-LPL$^{-/-}$ mice (*G*), whereas plasma insulin levels were unchanged (*H*). GFAP-LPL$^{-/-}$ mice had impaired glucose tolerance (*I*) and increased area under the curve (AUC) compared with their GFAP-LPL$^{+/+}$ littermates (*J*). White squares, GFAP-LPL$^{+/+}$ mice; black squares, GFAP-LPL$^{-/-}$ mice. *P < 0.05; **P < 0.01; ***P < 0.001; ****P < 0.0001. A total of 6–12 mice were used for the metabolic phenotyping and calorimetric study. BG, blood glucose.

metabolic control. We first found that LPL expression is increased in the hypothalami of mice fed an HFD over the long term, suggesting a potential role of LPL in the pathology of diet-induced obesity. We also found that LPL is more abundant in astrocytes than in neurons, consistent with the classic view that CNS astrocytes actively consume lipids. We found that LPL controls lipid storage in astrocytes in response to different nutrient inputs. A lack of LPL in astrocytes resulted in exaggerated body weight gain and glucose intolerance in animals fed the HFD, and these phenotypes were associated with increased ceramide content in the hypothalamus. These results indicate that astrocytes play a key role in sensing TGs and controlling lipid homeostasis.

We found that the LPL level in astrocytes varies according to the amount and specific mix of extracellular lipids. LPL was downregulated in the presence of TGs and palmitic acid, but upregulated by oleic acid. These data suggest that LPL may protect astrocytes from saturated fatty acid overload, an essential regulatory function for astrocytes to function properly during HFD-induced hyperlipidemia.

Moreover, we also observed increased ceramide content in the hypothalamus of mice lacking astrocytic LPL, consistent with studies indicating that the inhibition of LPL activity triggers de novo ceramide synthesis (29). In our study, we found that the deletion of LPL from astrocytes resulted in ceramide accumulation in hypothalamic neurons. Given that astrocytes metabolically supply lipids to neurons (9,33), we cannot rule out that the LPL deficiency in astrocytes might also cause the reduction of neuronal fatty acid availability, triggering de novo ceramide synthesis in neurons, as we observed. In our mouse model, we also found changes in AGRP immunoreactivity in the hypothalamus that might be a consequence of reduced lipid storage in the microenvironment as a result of the LPL deletion in astrocytes. Indeed, Libby et al. (34) reported that LPL is able to modulate AGRP level by regulating lipid storage in neurons. In addition to ceramide-induced lipid toxicity, we also observed elevation of ER stress markers and increased microglial immunoreactivity in the hypothalamus, both of which are associated with ceramide accumulation, as reported in other studies (31,32). Thus, these data suggest that disrupted lipid uptake in astrocytes causes ceramide to accumulate and consequentially contributes to the pathology of obesity.

Compared with a previous study using a neuronal LPL knockout approach (12), our astrocytic LPL-knockout mouse model had unchanged body weight when consuming a chow diet. Given that LPL is highly expressed in the infant rat brain during the lactating period and is reduced dramatically after weaning (35), we induced the deletion of LPL in adult mice to avoid developmental complications. Moreover, this deletion was restricted to GFAP-expressing astrocytes, which induced mainly changes in the hypothalamus rather than other brain areas, in order to investigate the significance of LPL function in these glial cells in the adult stage.

Overall, our data highlight the role of astrocytic lipid uptake in energy homeostasis. Mice lacking LPL in astrocytes have disrupted lipid metabolism in astrocytes and ceramide accumulation in hypothalamic neurons, contributing to impaired glucose tolerance and accelerated body weight gain in animals fed an HFD.

Acknowledgments. The authors thank Carola Meyer and Elma Stapic (Helmholtz Diabetes Center) for organizing the animal work. The authors also appreciate support from animal facility staff at University of Cincinnati (Metabolic Disease Institute) and the Helmholtz Diabetes Center.

Funding. This work was supported in part by funding from the Alexander von Humboldt Foundation (to M.H.T.), the Helmholtz ICEMED (Imaging and Curing Environmental Metabolic Diseases) Alliance and the Helmholtz Initiative on Personalized Medicine (iMed) through the Helmholtz Association, and the Helmholtz cross-program topic "Metabolic Dysfunction." This work also was supported by funding from the European Research Council (AdG HypoFlam no. 695054) and the Academisch Medisch Centrum (AMC) Fellowship (2014).

Duality of Interest. No conflicts of interest relevant to this article were reported.

Author Contributions. Y.G. performed the study, researched the data, analyzed results, and wrote the manuscript. Y.G., E.L., V.S.M., C.C.-G., C.M., S.L., R.H.E., C.-X.Y., C.G.-C., and M.H.T. designed the project and participated in the discussion. C.L. and B.L. performed the experiments. T.O.E. performed the lipidomics analysis. S.C.W. drafted the manuscript. C.G.-C. drafted the manuscript and contributed to performing all in vivo experiments. M.H.T. conceptualized and designed the project, interpreted the findings, and drafted the manuscript. M.H.T. is the guarantor of this work and, as such, had full access to all the data in the study and takes responsibility for the integrity of the data and the accuracy of the data analysis.

References

1. Clément L, Cruciani-Guglielmacci C, Magnan C, et al. Intracerebroventricular infusion of a triglyceride emulsion leads to both altered insulin secretion and hepatic glucose production in rats. Pflugers Arch 2002;445:375–380

2. Cruciani-Guglielmacci C, Hervalet A, Douared L, et al. Beta oxidation in the brain is required for the effects of non-esterified fatty acids on glucose-induced insulin secretion in rats. Diabetologia 2004;47:2032–2038

3. Lam TK, Pocai A, Gutierrez-Juarez R, et al. Hypothalamic sensing of circulating fatty acids is required for glucose homeostasis. Nat Med 2005;11:320–327

4. López M, Lelliott CJ, Vidal-Puig A. Hypothalamic fatty acid metabolism: a housekeeping pathway that regulates food intake. BioEssays 2007;29:248–261

5. Obici S, Feng Z, Morgan K, Stein D, Karkanias G, Rossetti L. Central administration of oleic acid inhibits glucose production and food intake. Diabetes 2002;51:271–275

6. Oomura Y, Nakamura T, Sugimori M, Yamada Y. Effect of free fatty acid on the rat lateral hypothalamic neurons. Physiol Behav 1975;14:483–486

7. Azevedo FA, Carvalho LR, Grinberg LT, et al. Equal numbers of neuronal and nonneuronal cells make the human brain an isometrically scaled-up primate brain. J Comp Neurol 2009;513:532–541

8. Edmond J. Energy metabolism in developing brain cells. Can J Physiol Pharmacol 1992;70(Suppl.):S118–S129

9. Le Foll C, Dunn-Meynell AA, Miziorko HM, Levin BE. Regulation of hypothalamic neuronal sensing and food intake by ketone bodies and fatty acids. Diabetes 2014;63:1259–1269

10. Edmond J, Robbins RA, Bergstrom JD, Cole RA, de Vellis J. Capacity for substrate utilization in oxidative metabolism by neurons, astrocytes, and oligodendrocytes from developing brain in primary culture. J Neurosci Res 1987;18:551–561

11. Horvath TL, Sarman B, García-Cáceres C, et al. Synaptic input organization of the melanocortin system predicts diet-induced hypothalamic reactive gliosis and obesity. Proc Natl Acad Sci U S A 2010;107:14875–14880

12. Wang H, Astarita G, Taussig MD, et al. Deficiency of lipoprotein lipase in neurons modifies the regulation of energy balance and leads to obesity. Cell Metab 2011;13:105–113
13. Fielding BA, Frayn KN. Lipoprotein lipase and the disposition of dietary fatty acids. Br J Nutr 1998;80:495–502
14. Wang H, Eckel RH. Lipoprotein lipase: from gene to obesity. Am J Physiol Endocrinol Metab 2009;297:E271–E288
15. Huey PU, Marcell T, Owens GC, Etienne J, Eckel RH. Lipoprotein lipase is expressed in cultured Schwann cells and functions in lipid synthesis and utilization. J Lipid Res 1998;39:2135–2142
16. Nishitsuji K, Hosono T, Uchimura K, Michikawa M. Lipoprotein lipase is a novel amyloid beta (Abeta)-binding protein that promotes glycosaminoglycan-dependent cellular uptake of Abeta in astrocytes. J Biol Chem 2011;286:6393–6401
17. Wang H, Eckel RH. Lipoprotein lipase in the brain and nervous system. Annu Rev Nutr 2012;32:147–160
18. Augustus A, Yagyu H, Haemmerle G, et al. Cardiac-specific knock-out of lipoprotein lipase alters plasma lipoprotein triglyceride metabolism and cardiac gene expression. J Biol Chem 2004;279:25050–25057
19. Ganat YM, Silbereis J, Cave C, et al. Early postnatal astroglial cells produce multilineage precursors and neural stem cells in vivo. J Neurosci 2006;26:8609–8621
20. Nolte C, Matyash M, Pivneva T, et al. GFAP promoter-controlled EGFP-expressing transgenic mice: a tool to visualize astrocytes and astrogliosis in living brain tissue. Glia 2001;33:72–86
21. Fischer J, Beckervordersandforth R, Tripathi P, Steiner-Mezzadri A, Ninkovic J, Götz M. Prospective isolation of adult neural stem cells from the mouse subependymal zone. Nat Protoc 2011;6:1981–1989
22. Gao Y, Ottaway N, Schriever SC, et al. Hormones and diet, but not body weight, control hypothalamic microglial activity. Glia 2014;62:17–25
23. Folch J, Lees M, Sloane Stanley GH. A simple method for the isolation and purification of total lipides from animal tissues. J Biol Chem 1957;226:497–509
24. Knittelfelder OL, Weberhofer BP, Eichmann TO, Kohlwein SD, Rechberger GN. A versatile ultra-high performance LC-MS method for lipid profiling. J Chromatogr B Analyt Technol Biomed Life Sci 2014;951-952:119–128
25. Eckel RH, Robbins RJ. Lipoprotein lipase is produced, regulated, and functional in rat brain. Proc Natl Acad Sci U S A 1984;81:7604–7607
26. Nimmerjahn A, Kirchhoff F, Helmchen F. Resting microglial cells are highly dynamic surveillants of brain parenchyma in vivo. Science 2005;308:1314–1318
27. Ding Z, Maubach G, Masamune A, Zhuo L. Glial fibrillary acidic protein promoter targets pancreatic stellate cells. Dig Liver Dis 2009;41:229–236
28. Tennakoon AH, Izawa T, Wijesundera KK, et al. Analysis of glial fibrillary acidic protein (GFAP)-expressing ductular cells in a rat liver cirrhosis model induced by repeated injections of thioacetamide (TAA). Exp Mol Pathol 2015;98:476–485
29. Picard A, Rouch C, Kassis N, et al. Hippocampal lipoprotein lipase regulates energy balance in rodents. Mol Metab 2013;3:167–176
30. Chavez JA, Summers SA. A ceramide-centric view of insulin resistance. Cell Metab 2012;15:585–594
31. Holland WL, Bikman BT, Wang LP, et al. Lipid-induced insulin resistance mediated by the proinflammatory receptor TLR4 requires saturated fatty acid-induced ceramide biosynthesis in mice. J Clin Invest 2011;121:1858–1870
32. Contreras C, González-García I, Martínez-Sánchez N, et al. Central ceramide-induced hypothalamic lipotoxicity and ER stress regulate energy balance. Cell Rep 2014;9:366–377
33. Guzmán M, Blázquez C. Is there an astrocyte-neuron ketone body shuttle? Trends Endocrinol Metab 2001;12:169–173
34. Libby AE, Wang H, Mittal R, Sungelo M, Potma E, Eckel RH. Lipoprotein lipase is an important modulator of lipid uptake and storage in hypothalamic neurons. Biochem Biophys Res Commun 2015;465:287–292
35. Tavangar K, Murata Y, Patel S, et al. Developmental regulation of lipoprotein lipase in rats. Am J Physiol 1992;262:E330–E337